CHEMICAL ANALYSIS

A SERIES OF MONOGRAPHS ON ANALYTICAL CHEMISTRY
AND ITS APPLICATIONS

Series Editor
J. D. WINEFORDNER

Volume 174

A complete list of the titles in this series appears at the end of this volume.

IN VIVO *GLUCOSE SENSING*

Edited by

DAVID D. CUNNINGHAM
JULIE A. STENKEN

WILEY
A JOHN WILEY & SONS, INC., PUBLICATION

CHAPTER 15

SURFACE-ENHANCED RAMAN SPECTROSCOPY FOR GLUCOSE SENSING

Nilam C. Shah, Jonathan M. Yuen, Olga Lyandres, Matthew R. Glucksberg, Joseph T. Walsh and Richard P. Van Duyne

In Vivo Glucose Sensing, Edited by David D. Cunningham and Julie A. Stenken
Copyright © 2010 John Wiley & Sons, Inc.

15.1 BACKGROUND

15.1.1 Introduction

Frequent monitoring of glucose levels is critically important to the management of diabetes and reduction of complications. The detection of glucose is a highly researched area in the quest for a sensor that can give direct, real-time measurements, accurately, in real time, with minimum invasiveness. Several optical techniques are being explored for glucose detection, including infrared spectroscopy, polarimetry, polyacrylamide hydrogels, and photonic crystals.[1–5] However, there are limitations to these techniques including interfering water absorption, overlapping signals from competing analytes, and complications from indirect measurement. Surface-enhanced Raman spectroscopy (SERS) offers an alternative approach to detecting glucose that can overcome these limitations. Previously SERS has not been widely used for bioanalysis due to several factors including the requirement that molecules should be within a few nanometers of a roughened metal surface and the spectral complexity of biological media. While the use of SERS-active labels resulted in successful detection of proteins and antigens *in vitro*,[6–8] *in vivo* direct detection of bioanalytes remains a challenge. This chapter outlines the development of a sensitive, portable, robust SERS-based glucose sensor that overcomes many of the obstacles related to using SERS to detect bioanalytes. We start with a simplified *in vitro* scheme to examine fundamental properties of the glucose sensor such as reversibility, stability, and temporal response. Then, we demonstrate quantitative detection of glucose in an aqueous environment and in a simulated biological environment (i.e., bovine plasma). Furthermore, we show successful quantitative detection of glucose *in vivo* by implanting a SERS substrate into the interstitial space of a rat. Finally, we compare the SERS-based glucose sensor to a commercially available glucose sensor.

15.1.2 Raman Spectroscopy

When light interacts with molecules, it is either absorbed, transmitted, or scattered. The scattered component can either be elastic (i.e., Rayleigh) or inelastic (i.e., Raman). Raman scattered photons are shifted in frequency from the incident photons by the amount of energy transferred to the molecule to excite its vibrational modes. This process is referred to as normal Raman scattering (NRS). The normal Raman spectrum is a plot of the intensity of Raman scattered light versus the energy difference between incident and scattered photons and is extremely sensitive to the molecular structure of the target molecule.[9] The individual bands in a normal Raman spectrum are characteristic of specific vibrational motions. As a result, every molecular species has its own unique Raman spectrum. This molecular specificity of Raman spectroscopy is utilized to create a glucose sensor. The molecular specificity of NRS for six common metabolic analytes found in the interstitial space is clearly illustrated in Figure 15.1. For example, analytes whose molecular structures differ only in the position of a single atom like glucose (Figure 15.1, upper left) and galactose (Figure 15.1, middle left) are easily distinguished. Even more

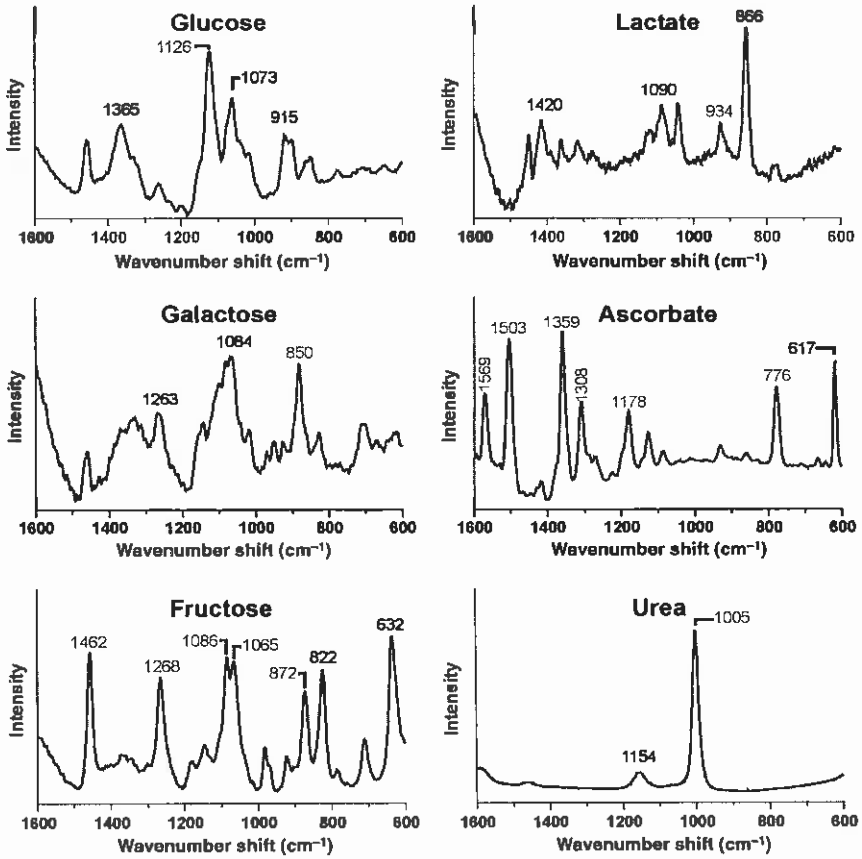

Figure 15.1 Raman spectra of common metabolic analytes of the interstitium. Saturated aqueous solutions, $\lambda_{ex} = 532$ nm, $P = 30$ mW, and $t = 2$ min.

dramatic is the ability to distinguish between isomers such as glucose (Figure 15.1, upper left) and fructose (Figure 15.1, lower left), providing significant selectivity with the analysis.

The application of Raman spectroscopy to the measurement of glucose is not new. It has been shown that normal Raman spectroscopy can readily detect physiological concentrations of glucose *in vitro* from a simulated aqueous humor solution.[10] Using partial least squares (PLS) analysis, Lambert et al. were able to predict glucose levels ranging from 50 mg/dL (2.8 mM, hypoglycemic) to 1300 mg/dL (72.2 mM, severe diabetic) with a standard error of 24.7 mg/dL (1.4 mM). Berger et al. were able to detect glucose concentrations with an accuracy of 26 mg/dL (1.4 mM) in serum and 79 mg/dL (4.4 mM) in whole blood using PLS.[11] These are promising results and show the potential of Raman spectroscopy for glucose measurements; unfortunately, the light exposure in both experiments was significantly higher than is permissible in a biological specimen.[12] High-power lasers (100–300 mW) and long acquisition times

(as long as 5 min) are required because of the small normal Raman scattering cross section of glucose, 5.6×10^{-30} cm^2/molecule/stearadians.[9]

The Raman scattering cross section for one of the most intense vibrational modes known, the $n1$ totally symmetric ring breathing mode of liquid benzene, is only 1.06×10^{-29} cm^2/molecule/stearadian. Since glucose has an even smaller normal Raman scattering cross section, due to the extremely weak interaction between an input (viz., excitation) photon and the analyte molecule, the signal will be weak. Thus, to get adequate signal-to-noise, NRS requires relatively high concentrations, high laser power (100–300 mW), and long integration times (as long as 5 min). Typically, the limit of detection (LOD) for NRS is of order 10–100 mM. Ongoing efforts to develop Raman technology for noninvasive glucose sensing are presented in the Chapter 14.

Raman optical activity (ROA) spectroscopy is highly sensitive to structural changes, while Raman difference spectroscopy is capable of detecting small differences in Raman signal at low concentrations of analytes. In both these techniques, however, the resultant difference signals are very small and long data acquisition times are required if signals from physiologic concentrations of analytes are to be obtained with precision or accuracy.[13,14] Therefore, these approaches are not ideal for a rapid, robust, and clinical analysis.

One solution to overcome the low signal intensity of NRS is to use resonance Raman spectroscopy (RRS), which can increase the Raman cross section. In RRS the excitation wavelength of the incident light is chosen to be coincident with an intense molecular electronic absorption transition (viz., chromophore) in the target molecule. RRS works extremely well for heme proteins such as cytochrome *c* using visible light and for direct excitation of amino acids in proteins using ultraviolet light. RRS has been proven to be a powerful tool in biology for examining protein structure. Furthermore, in its time-resolved variant, it is one of the few biophysical techniques capable of structural insight into the femtosecond timescale. The sensitivity enhancement factors associated with RRS can be as large as 10^4–10^5 so that the typical LOD for RRS can be as low as 10^{-6}–10^{-5} M. Unfortunately, glucose has no visible or accessible ultraviolet chromophores and would require excitation in the deep ultraviolet region ($\lambda_{ex} \sim 200$ nm) of the spectrum. Ultraviolet excitation is unlikely to be appropriate for *in vivo* sensing due to photodamage of DNA and absorption by water.

Another solution to the insensitivity of NRS was discovered by Van Duyne in 1977 and is known as SERS.[15] When an analyte molecule is adsorbed on or is located within 0–2 nm of a roughened silver or gold metal surface, the intensity of normal Raman scattering by the molecule can be amplified by enhancement factors of 10^6–10^8. In the case of resonant analyte molecules, the combined SERS and RRS enhancement factors can be as high as 10^{14}–10^{15} for single molecules and is known as surface-enhanced resonance Raman scattering (SERRS). Although the details of the enhancement mechanism(s) responsible for such large enhancements are not yet understood,[16–18] recent experiments have shown that by careful control of nanoparticle structure, the SERS enhancement factors due to the electromagnetic enhancement mechanism may be increased to at least 10^8 for nonresonant adsorbates and to 10^{10}–10^{15} for resonant adsorbates.[19] SERS is most intense on silver, but other metals, such as copper and gold, also function well as SERS-active surfaces. SERS signals are optimized when the energy of the localized surface plasmon resonance (LSPR) lies within the energy range of the Raman scattered photons. Excitation of the LSPR excites the conduction band electrons of the metal. The oscillating electrons set up an amplified electromagnetic field surrounding the nanostructured surface. Molecules affected by the local electromagnetic field exhibit stronger Raman excitation and scattering probabilites.[20]

15.1.3 Localized Surface Plasmon Resonance

The signature optical property of a noble metal nanostructure is the LSPR. This resonance occurs when the correct wavelength of light strikes a noble metal nanostructure, causing the plasma of conduction band electrons to oscillate collectively. The term LSPR is used to emphasize that this collective oscillation is localized near the surface of the nanoparticle and to differentiate it from propagating surface plasmons that are referred to simply as surface plasmons. The two consequences of LSPR excitation are (1) selective photon absorption and (2) generation of locally enhanced or amplified electromagnetic fields at the nanoparticle surface. The wavelength of the LSPR depends on many factors including the material, size, shape, spacing, and dielectric environment of the nanoparticle. Many research groups are currently exploring the size-dependent optical properties of noble metal nanoparticles to exploit LSPR in applications with optical filters,[21,22] substrates for surface-enhanced spectroscopies,[23–34] biosensors,[35–37] bioprobes,[38,39] chemical sensors,[40,41] and optical devices.[40–45] The LSPR for noble metal nanoparticles in the twenty to few hundred nanometer size range occurs in the visible and IR regions of the spectrum and can be measured by UV–visible–IR extinction spectroscopy.[46] The resulting SER spectrum is related intricately to the spectral location of the LSPR. We have previously shown that we can fabricate nanostructured surfaces with the LSPR matched to the excitation wavelength using nanosphere lithography.[47] An atomic force micrograph of a nanostructured surface with the LSPR matched to 785 nm excitation is shown in Figure15.2. This structure consists of silver film-over-nanospheres (AgFON) on a copper substrate. The fabrication procedure of these substrates is described below.

15.1.4 Nanosphere Lithography

Nanosphere lithography (NSL) is an inexpensive fabrication technique developed in the Van Duyne lab to produce nanoparticle arrays with precisely controlled shape, size, and interparticle spacing, and—accordingly—precisely controlled LSPRs.[48] The production of nanoparticles by NSL begins with the self-assembly of size-monodispersed nanospheres to form a two-dimensional colloidal crystal deposition mask: nanospheres are deposited on the substrate surface, allowed to diffuse freely, seek their lowest energy conformation, and as the solvent evaporates the nanospheres are drawn together in a hexagonally close-packed pattern (Figure15.3a). Following self-assembly of the nanosphere mask, a noble metal or other material is deposited by thermal evaporation, electron beam deposition (EBD), or pulsed laser

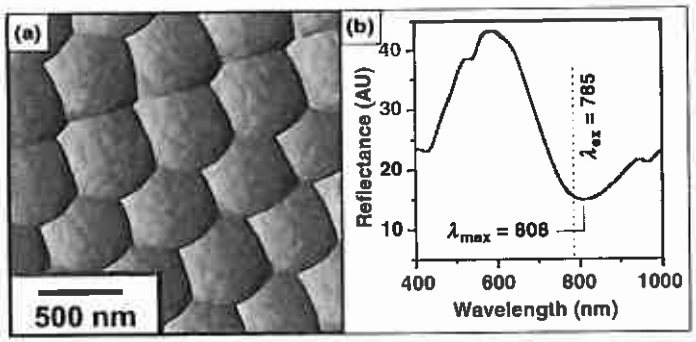

Figure 15.2 (a) Atomic micrograph of silver film-over-nanospheres (AgFON). (b) Reflectance spectrum of the AgFON nanostructure optimized with the LSPR matched to 785 nm excitation.

deposition (PLD) from a source normal to the substrate through the nanosphere mask to a controlled mass thickness (typically in the range of 20–80 nm). Subsequently, the nanosphere mask is removed by sonicating the entire sample in a solvent, thus leaving behind nanoparticles. The tetrahedral nanoparticles are shown in Figure15.3b, deposited through the nanosphere mask on to the substrate. Previous work has demonstrated that the LSPR of NSL-derived nanoparticles depends on nanoparticle material, size, shape, and interparticle spacing as well as substrate, solvent, dielectric thin-film overlayers, and molecular adsorbates.[46] The size of these nanoparticles is easily tuned to have a peak LSPR that matches the excitation source. NSL can be used to produce monodispersed, reproducible, and material-general nanoparticles. Tetrahedral Ag nanoparticle arrays produce enhancement factors on the order of 10^8.[19,49] NSL can also be utilized to fabricate many new nanostructure derivatives such as silver film-over-nanospheres (AgFONs), which are used for the glucose sensor (Figure15.2). AgFONs exhibit enhancement factors on the order of 10^7.[47] However, AgFONs have a significant increase in surface area accessible to analyte molecules increasing the total signal intensity and making them more suitable for glucose sensing. AgFONs are fabricated by depositing a layer of metal

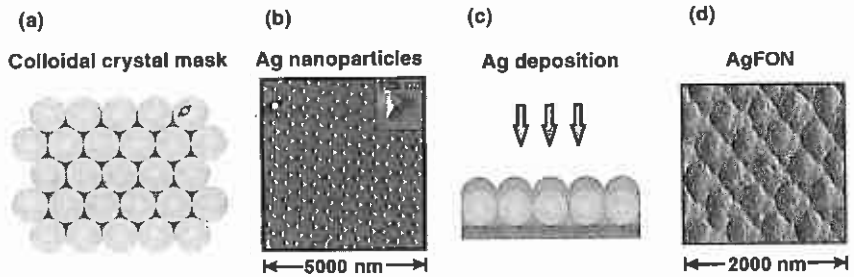

Figure 15.3 (a) Depiction of nanosphere monolayer, (b) atomic force micrograph of resulting tetrahedral nanoparticle array formed after deposition of metal and removal of nanospheres, (c) schematic of AgFON fabrication, and (d) an atomic force micrograph of the AgFON.

over the nanosphere mask with mass thickness of approximately a half of the sphere diameter as shown in Figure15.3c. The metal is deposited through and over the spheres such that the Ag film is in contact with the supporting substrate. These contacts serve as heat sinks for the surface and prevent photothermal damage to the surface. The resulting surface (Figure15.3d) can then be functionalized and used for SERS sensing.

15.1.5 Partitioning of Glucose

When a Raman-active molecule is located close to nanostructured noble metal surfaces, the ensemble-averaged Raman signal increases by up to eight orders of magnitude[49] for nonresonant molecules. Under some conditions, the Raman signal from single molecules can be enhanced by 14 or 15 orders of magnitude in the case of resonant adsorbates.[17,18] Theoretical analysis suggests that molecules confined within the decay length of the electromagnetic fields, namely, 0–2 nm, will exhibit SER spectra even if they are not chemisorbed.[20] For the SERS-active surfaces used in glucose detection, the decay length at which the intensity decreases by a factor of 10 was calculated to be 2.8 nm.[47] SERS possesses many desirable characteristics as a tool for the chemical analysis of *in vivo* molecular species including high specificity, attomole to high zeptomole mass sensitivity, micromolar to picomolar concentration sensitivity, and interfacial generality;[50] however, glucose affinity to bare metal surfaces is low. Therefore, it is essential to partition glucose close to the surface to detect it with SERS. To increase the number of probed glucose molecules, we need to facilitate their interaction with the metal surface by using a self-assembled monolayer (SAM), in a manner analogous to high-performance liquid chromatography (HPLC).[51–55] In addition, the partition layer also needs to bind glucose reversibly such that the fluctuations in glucose levels can be reflected accurately and the sensor does not saturate within the physiological concentration range. We have explored several different partition layers to increase the interaction of glucose with the metal surface and to ensure reversible binding of glucose.

Our early work indicated that decanethiol (DT)[56] and tri(ethylene glycol)-terminated alkanethiol (EG3)[57] would be promising partition layers. However, upon further investigation it was found that DT was hydrophobic and not compatible with an aqueous environment, while EG3 is a challenge to synthesize, making its availability limited. Recently, a new mixed monolayer, consisting of DT and mercaptohexanol (MH), has been explored.[58] This mixed DT/MH SAM has dual hydrophobic and hydrophilic properties that make it ideal for *in vivo* use. Figure15.4a depicts the steps involved in making the DT/MH-functionalized AgFON. We hypothesize, using a space-filling model, that the DT/MH SAM creates a pocket that brings glucose closer to the noble metal surface, thus enhancing the SERS signal (Figure15.4b). A SERS spectrum of the DT/MH AgFON is shown in Figure15.4c. We have demonstrated reversibility, stability, rapid time response, and quantitative detection of glucose with the DT/MH SAM both *in vitro* and *in vivo* as detailed below.

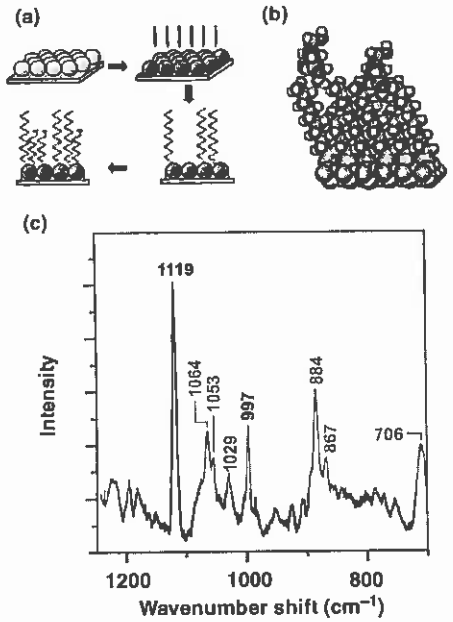

Figure 15.4 Decanethiol/mercaptohexanol-functionalized AgFON fabrication, space-filling model, and spectrum. (a) AgFONs were prepared by depositing a film of metal onto a layer of self-assembled nanospheres. The AgFON was then functionalized by incubating in ethanolic solutions of mercaptohexanol for 45 min and then in decanethiol overnight. (b) Space-filling model of glucose partitioning into the DT/MH-functionalized AgFON. (c) SERS spectrum of a DT/MH-functionalized AgFON. $\lambda_{ex} = 785$ nm, $P = 55$ mW, and $t = 2$ min.

15.2 EXPERIMENTAL PROCEDURES

15.2.1 AgFON Substrate Preparation

Copper 18 mm diameter discs were utilized as substrates for glucose detection. After cleaning, approximately 10 μL of the nanosphere suspension (4% solids, 390 nm diameter) was drop coated onto each copper substrate and allowed to dry in ambient conditions.[58] The substrates were then mounted into an electron beam deposition system for metal deposition (Kurt J. Lesker, Clairton, PA). Silver metal films ($d_m = 200$ nm) were deposited over and through the sphere masks on the substrates.[58,59]

The AgFON surfaces were then functionalized with a SAM composed of decanethiol and mercaptohexanol. The AgFONs were first incubated in 1 mM DT in ethanol for 45 min and then transferred to 1 mM MH in ethanol for at least 12 h. The SAM-functionalized surfaces were then mounted into a small-volume flow cell for SERS measurements.

15.2.2 SERS Apparatus

A titanium–sapphire laser (CW Ti:Sa, model 3900, Spectra Physics, Mountain View, CA) pumped by a solid-state diode laser, λ_{ex} 532 nm (model Millenia Vs, Spectra Physics) was used to generate λ_{ex} of 785 nm as described previously.[58] The setup consisted of laser line and high-pass filters for the corresponding wavelengths used. Furthermore, a lens was used to focus the beam onto the sample and a collection lens was used to focus scattered light onto the entrance slit of the single-grating monochromator (Acton Research Scientific, Trenton, NJ). For initial studies of reversibility, stability, and time response of the sensor, 532 nm excitation was used. For all *in vivo* studies, and *in vitro* studies conducted in a biological environment (such as plasma), 785 nm excitation was used because NIR excitation minimizes autofluorescence of proteins.[58] A small-volume flow cell was used to control the external environment of the AgFON surfaces.

15.2.3 Quantitative Multivariate Analysis

All data processing was performed using MATLAB (MathWorks, Inc., Natick, MA) and PLS_Toolbox (Eigenvector Research, Inc., Manson, WA). Prior to analysis, the spectra were smoothed with a second-order polynomial and window size of 9. The slowly varying background, commonly seen in SERS experiments, was removed by subtracting a fourth-order polynomial fit. This method greatly reduced varying background levels with minimum effect on the SERS peaks. Chemometric analysis was performed using the PLS method and leave-one-out (LOO) cross-validation algorithm.[57,60] PLS is an inverse calibration method that does not require *apriori* knowledge of all the components in the system.[61] To construct the calibration, known concentrations of the analyte are used. The regression vector, **b**, is then determined based on the spectra matrix, **R**, and concentration of the training set, **c**:

$$\mathbf{c} = \mathbf{Rb}$$

The regression vector shows the vibrational features of the analyte (in our case glucose) and is used to predict the concentration of an unknown sample.

To calibrate the SERS sensor, a training set was acquired that consisted of spectra of solutions with glucose concentration in the physiological range (10–450 mg/dL). The root mean square error of calibration (RMSEC) was calculated to gauge how well the data fit the calibration model. To further ensure a valid model, it is important to test the calibration model with an independent validation set.[61] Once an independent validation set of spectra was acquired, the resulting regression vector was used to predict concentrations. Finally, the root mean squared error of prediction (RMSEP) was calculated to gauge the accuracy of the prediction.

15.2.4 Temporal Response Analysis

At the conclusion of an experiment, a DT/MH-functionalized AgFON was removed after being incubated in bovine plasma or implanted in the rat for 5 h and placed in a flow cell containing bovine plasma to simulate the *in vivo* environment.

High and low concentrations of glucose dissolved in plasma were injected into the cell to cause step changes in glucose concentration. PeakFit 4.12 software (Systat Software Inc, Richmond, CA) was used to process the data. Using Matlab software a fourth-order polynomial was subtracted from the baseline SERS spectra to remove the background signal. A linear best-fit baseline correction and Savitzky–Golay smoothing were also applied in PeakFit. The data were fit to the superposition of the Lorentzian amplitude line shapes to determine the amplitude of the Raman bands. The data were then iteratively fit to an exponential curve to determine the $1/e$ time constant.

15.2.5 Surgical Implantation and Spectroscopic Measurements

All surgical procedures followed animal study protocols filed with Northwestern University's Institutional Animal Care and Use Committee (IACUC). Adult, male Sprague Dawley rats (300–500 g, $N = 4$) were anesthetized using Nembutal (sodium pentobarbital, Abbott Laboratories, Abbott Park, IL) with an initial dose of 50 mg/kg. Rats are an accepted animal model for metabolic disorders including diabetes.[62] They are also commonly used for experimental glucose measurements. Animal anesthesia was maintained by additional hourly administrations of Nembutal (25 mg/kg). After initial anesthetization, the animals were checked for pain responses by paw pinch and blink tests. No action was taken if responses were seen. The surgical areas were prepared by hair removal (shaving and chemical depilatory) and cleaning after the anesthetic had taken effect. Then, the femoral vein was cannulated using PE50 tubing (Clay Adams, Becton, Dickinson and Company, Franklin Lakes, NJ). The carotid artery was then cannulated with PE90 tubing. The venous cannula was used for glucose, saline, and other injections. A tracheotomy was performed and a tube inserted to enable the attachment of a ventilator to aid respiration. All incisions were shut with surgical clips. Throughout the surgery and the experiment, the rat was warmed using an electric heating pad. A glass window in a metal frame was placed along the midline of the back of the rat. A circular incision was made to all implantations of a DT/MH-functionalized AgFON sensor subcutaneously such that the substrate was in contact with the interstitial fluid and optically accessible through the window. The rat was then positioned within a holder in the conventional sample position on a lab-scale Raman spectroscopy system (Figure15.5). The system consisted of a monochromatic laser, a band-pass filter, a series of steering and focusing optics to deliver the laser light to the sample, and collection optics that convey the scattered light to the detector, a long-pass filter to reject Rayleigh scattering, a 3 m spectrograph for wavelength dispersion, and a CCD detector. Following IACUC protocol, at the conclusion of the experiment the animals were sacrificed by an overdose of anesthetic and bilateral thorachotomy.

Glucose levels in the rat were controlled through intermittent intravenous infusion for 3 h. The glucose was infused over 5–10 min at a concentration of 1 g/mL in sterile phosphate buffered saline via the femoral venous cannula. A small droplet of blood was drawn from the femoral arterial cannula, the glucose concentration was measured with the One Touch II glucometer (Lifescan, Inc.), and corresponding SERS measurements were taken. SERS spectra were acquired through the optical

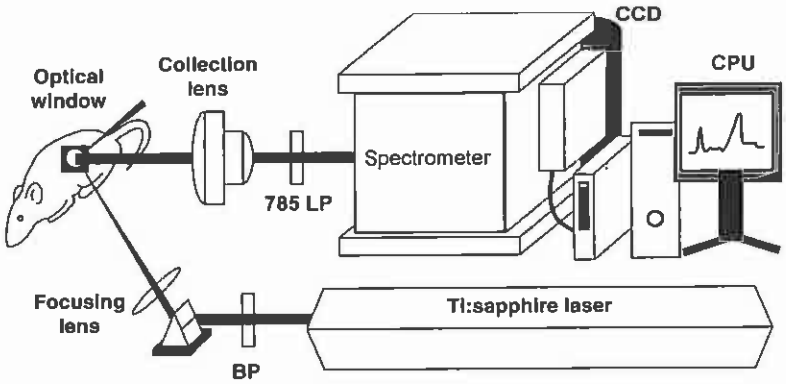

Figure 15.5 Schematic of instrumental apparatus. The DT/MH-functionalized AgFON was surgically implanted into a rat with an optical window and integrated into a conventional laboratory Raman spectroscopy system. The Raman spectroscopy system consists of a Ti: sapphire laser ($\lambda_{ex} = 785$ nm), band-pass filter, beam-steering optics, collection optics, and a long-pass filter to reject Raleigh scattered light. All of the optics fit on a 4 ft × 10 ft optical table.

window using a Ti:sapphire laser ($\lambda_{ex} = 785$ nm, $P = 50$ mW, and $t = 2$ min). The partial least squares method previously described was used to analyze the data collected.

15.3 RESULTS

The following results show considerable progress toward an implantable, real-time, continuous, SERS-based glucose sensor. Our work demonstrates the ability to detect glucose both *in vitro* and *in vivo* with SERS using a mixed SAM consisting of decanethiol and mercaptohexanol (DT/MH). We demonstrate (1) reversibility of the sensor, (2) long-term stability of the DT/MH-functionalized AgFON surface (3) real-time partitioning and departitioning of the glucose sensor, (4) quantitative measurements, and (5) comparison of the SERS-based sensor to electrochemical measurements.

15.3.1 Reversibility of the DT/MH AgFON

To successfully monitor fluctuations in glucose concentration throughout the day, an implantable glucose sensor must be reversible. The DT/MH-modified AgFON sensor was exposed to cycles of 0 and 100 mM aqueous glucose solutions (pH ~ 7) to demonstrate the reversibility of the sensor (Figure15.6). The sensor was not flushed between measurements to simulate real-time sensing. To minimize effective laser power fluctuations, nitrate was used as an internal standard (1053 cm^{-1} peak) in all the experiments. This band was used to normalize the spectra and corresponds to a symmetric stretching of NO_3^-.[63] SER spectra were collected at each step ($\lambda = 532$ nm, $P = 10$ mW, and $t = 20$ min) (Figure15.6a–c (left)).

The experimental spectra shown in Figure15.6 d–f (right) compare the experimental spectra to the normal Raman spectrum of a saturated aqueous glucose solution. Peaks at 1462, 1365, 1268, 1126, 915, and 850 cm^{-1} correspond to glucose peaks in the saturated solution (Figure15.6d).[64] In all the difference spectra, a sharp peak can be seen at 1053 cm^{-1}, representing imperfect subtraction of the nitrate internal standard. Figure15.6e demonstrates the partitioning of glucose in the DT/MH SAM with features at 1461, 1371, 1269, 1131, 916, and 864 cm^{-1}. The shift in the glucose peaks compared to the saturated solution is due to the fact that SERS bands can shift up to 25 cm^{-1} when compared to normal Raman bands of the same analyte.[65] Complete departitioning of glucose is represented by the absence of glucose spectral features in the difference spectra shown in Figure15.6f. The data demonstrate that the DT/MH-mixed SAM has a reversible sensing surface for optimal partitioning and departitioning of glucose.

15.3.2 Stability of DT/MH AgFON

An implantable glucose sensor must also be stable for a minimum of 3 days.[66] Previously, we demonstrated by electrochemical and SERS measurements that

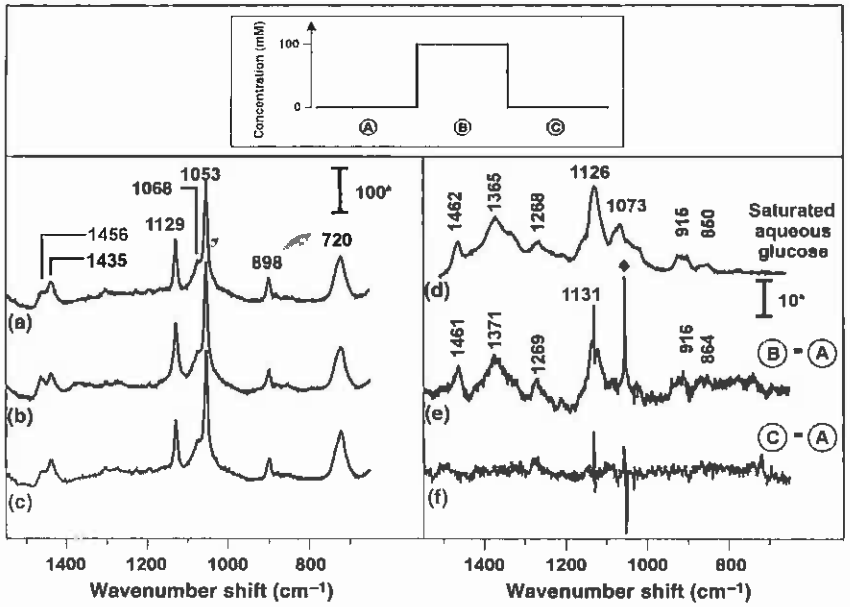

Figure 15.6 Inset shows the step changes in glucose concentration experienced by the sensor. (a, b, and c) SER spectra collected for each step for alternate 0 and 100 mM aqueous glucose solutions. (d) The normal Raman spectrum of aqueous saturated glucose solution. (e and f) Show the differences indicating glucose partitioning and departitioning. Raman bands in the difference spectra showing partitioning of glucose (e) agree well with the reference glucose spectrum (d). The absence of spectral features in (f) indicates complete departioning of glucose. Symbol * denotes analog-to-digital units/mW/s. $\lambda_{ex} = 532$ nm, $P = 10$ mW, $t = 20$ min, and pH ~ 7.

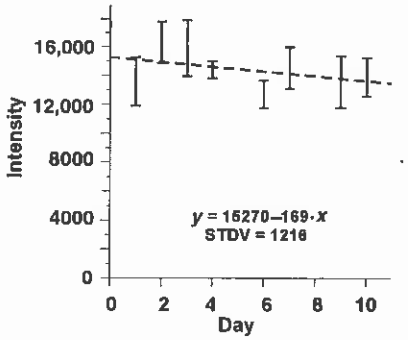

Figure 15.7 Stability of DT/MH-functionalized AgFON in bovine plasma. Plot depicts the intensity of the 1119 cm^{-1} peak versus time. Signal intensity stayed stable over a 10-day period with a 2% change in intensity of the 1119 cm^{-1} peak. STDV = 1216 counts, $\lambda_{ex} = 785$ nm, $P_{laser} = 55$ mW, and $t = 2$ min.

SAM-functionalized AgFON substrates were stable for at least 3 days in phosphate-buffered saline.[67] Here, we show 10 days stability of the DT/MH-functionalized AgFON surface in bovine plasma. SER spectra were taken once every 24 h on three different spots for three different samples ($\lambda = 785$ nm, $t = 2$ min). Figure15.7 gives the plot of the average intensity of the 1119-cm^{-1} peak for DT/MH on the AgFON, which corresponds to the stretching vibration of a C–C bond,[68] for each day as a function of time. The 1119 cm^{-1} peak was chosen because it gives a strong signal for the DT/MH SAM allowing fluctuations in intensity to be easily measured. From the first day to the last, only a 2% change in intensity was observed with a standard deviation (STDV) of 1216 counts. The change was seen as not significant and can be explained by the rearrangement of the SAM during the incubation in bovine plasma.[69] This experiment demonstrates that the DT/MH SAM is intact and well ordered over a 10-day period, making this SAM-functionalized surface a good candidate as an implantable sensor.

15.3.3 Temporal Response

In addition to reversibility and stability, the sensor must be able to partition and departition glucose on a reasonable timescale. The *in vitro* real-time response was examined by using bovine plasma. The DT/MH-functionalized AgFON was placed in bovine plasma for ~5 h. The AgFON substrate was then placed in a flow cell and SER spectra were collected continuously ($\lambda_{ex} = 785$ nm) with a 15 s integration time. Spectra were collected at 785 nm to reduce autoflourescence of proteins from the bovine plasma. To observe partitioning, bovine plasma (used as purchased) spiked with 50 mM glucose was injected at $t = 0$ s. Departitioning was observed by injecting 0 mM glucose in bovine plasma at $t = 225$ s. The amplitude of the 1462 cm^{-1} peak was plotted versus time as shown in Figure15.8a (top). An offset was subtracted from the data such that the first intensity value is zero. The $1/e$ time constant was calculated from an exponential curve fitted to the data points. The fit yields a $1/e$ time constant of 28 s for partitioning and 25 s for departitioning.[58]

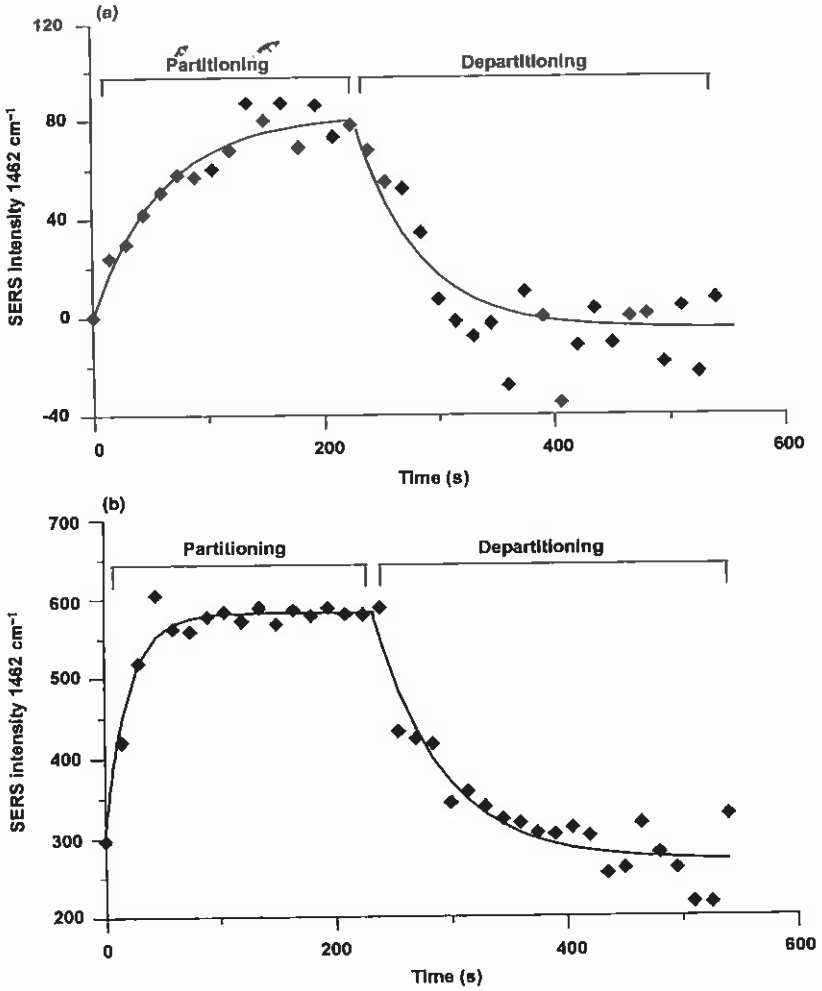

Figure 15.8 Real-time SERS response to a step change in glucose concentration. Glucose was injected at $t = 0$ s, and the cell was flushed with glucose-depleted bovine plasma at $t = 225$ s. ($\lambda_{ex} = 785$ nm, $P = 100$ mW, and $t = 15$ s) (a) Partitioning and departioning of glucose after being incubated in bovine plasma for ~5 h. The $1/e$ time constants were calculated to be 28 s for partitioning and 25 s for departitioning. (b) Partitioning and departitioning of glucose after being implanted in a rat for ~5 h. The $1/e$ time constants were calculated to be 9 s for partitioning and 27 s for departitioning.

A similar experiment was conducted after the sensor was implanted in the rat for ~5 h. This experiment was done to test whether implanting the sensor fouls the surface and alters the partitioning and departitioning of glucose. The sensor was removed from the rat and immediately placed in a flow cell containing bovine plasma to simulate the *in vivo* environment. The $1/e$ time constant was then determined as described above. In this case, the fit yields a $1/e$ time constant of 9 s for partitioning and 27 s for departitioning (Figure15.8b, bottom). These results indicate that changes in glucose concentration can be detected rapidly both *in vitro* and *in vivo*.

15.3.4 *In Vitro* Quantitative Detection

A viable glucose sensor must also be able to detect glucose in the clinically relevant concentration range, 10–450 mg/dL (0.56–25 mM), in the presence of interfering analytes, under physiological pH. Data are often presented on a Clarke error grid as described in Chapter 1. To evaluate the SERS-based glucose sensor against the Clarke error grid, the DT/MH-functionalized AgFON samples were placed in a flow cell containing water (pH ~ 7) with lactate (1 mM) and urea (2.5 mM) in physiological concentrations, which are potential interferences for glucose. Random concentrations of glucose solutions ranging from 10 to 450 mg/dL were then introduced into the cell and allowed to incubate for 2 min to ensure complete partitioning. A near-infrared laser source ($\lambda_{ex} = 785$ nm, $P = 8.4$ mW, and $t = 2$ min) was used to collect SER spectra from multiple locations on two substrates. The calibration model was constructed by partial least squares leave-one-out (PLS-LOO) analysis using 46 randomly chosen independent spectral measurements of known glucose concentrations. Seven latent variables were used as the basis for the calibration model. The variables take into account the environment in the laboratory, variation in laser power, and SERS enhancement at different locations. The number of latent variables that are used should be chosen carefully because using too many latent variables can result in overfitting of the data. Using a cross-validation step in the calibration process allows us to determine the number of latent variables to use. The number of latent variables is chosen by constructing a plot of root mean squared error of cross-validation (RMSECV) versus latent variables and finding the minimum RMSECV value.[61] The PLS analysis resulted in a RMSEC of 9.89 mg/dL (0.549 mM). This RMSEC value is lower than previously reported when using the EG3-modified AgFON. In order to validate the PLS model, 23 independent data points were used, resulting in a root mean square error of prediction (RMSEP) of 92.17 mg/dL (5.12 mM). As seen in Figure15.9, 98% of the calibration set and 87% of the validation set fall within the A and B ranges of the Clarke error grid.

The glucose sensor was then evaluated in bovine plasma to simulate the *in vivo* environment. The bovine plasma was passed through a 0.45 μm diameter pore filter before use, and then spiked with glucose concentrations from 10 to 450 mg/dL. DT/MH-functionalized AgFON substrates were placed in the flow cell and allowed to incubate in the glucose-spiked bovine plasma. SERS spectra were collected from multiple spots and multiple samples at various random glucose concentrations ($\lambda = 785$ nm, $P = 10$–30 mW, and $t = 2$ min). The calibration model was constructed with 92 data points using PLS-LOO with seven latent variables. The analysis resulted in an RMSEC of 34.3 mg/dL (1.90 mM). The model was validated by using 46 data points, resulting in an RMSEP of 83.16 mg/dL (4.62 mM). Plotting the data demonstrated that 98% of the calibration set and 85% of the validation set fall within the A and B ranges of the Clarke error grid (Figure15.10). The results indicate that the DT/MH-modified AgFON glucose sensor can make accurate glucose measurements *in vitro* even in the presence of interfering analytes.

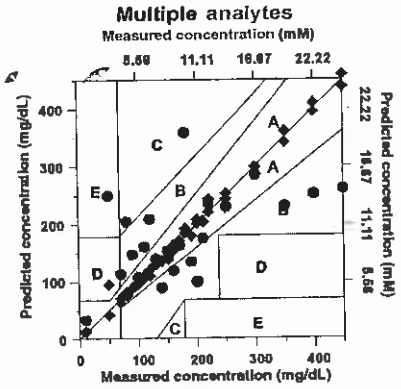

Figure 15.9 Calibration (◆) and validation (●) plot of glucose in an aqueous solution consisting of 1 mM lactate and 2.5 mM urea at pH ~ 7 on a DT/MH-functionalized AgFON surface. Two substrates and multiple spots were used to measure glucose concentrations in the physiological range (10–450 mg/dL). The calibration plot was constructed using 46 data points with PLS-LOO analysis. The validation plot was constructed using 23 data points. RMSEC 9.89 mg/dL (0.55 mM) and RMSEP = 92.17 mg/dL (5.12 mM). $\lambda_{ex} = 785$ nm, $P_{laser} = 8.4$ mW, and $t = 2$ min.

15.3.5 *In Vivo* Detection

Finally, the DT/MH AgFON was evaluated *in vivo*. A representative Clarke error grid analysis of a single rodent is shown in Figure15.11. All measurements were taken from a single spot on the implanted DT/MH-functionalized AgFON surface.

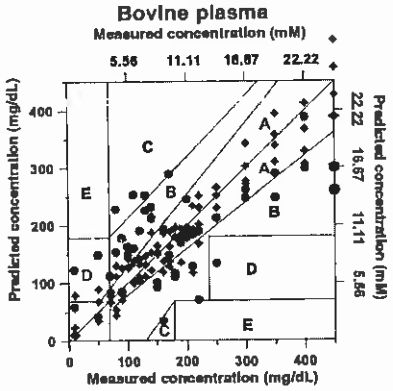

Figure 15.10 Calibration (◆) and validation (●) plot of glucose in bovine plasma on a DT/MH-functionalized AgFON surface. Three substrates and multiple spots were used to measure glucose concentrations in the physiological range (10–450 mg/dL) over the course of 2 days. PLS calibration plot was constructed using 92 data points. The validation plot was constructed using 46 data points. RMSEC = 34.3 mg/dL (1.9 mM) and RMSEP = 83.16 mg/dL (4.62 mM). $\lambda_{ex} = 785$ nm, $P_{laser} = 10$–30 mW, and $t = 2$ min.

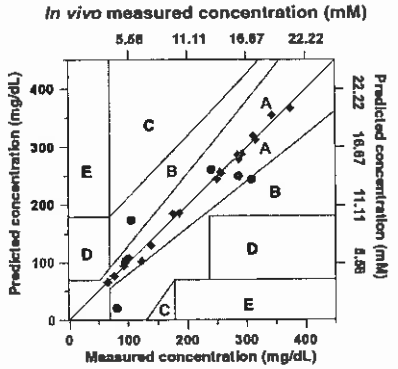

Figure 15.11 Calibration (◆) and validation (●) plot using a single sensor and a single spot on a DT/MH-functionalized AgFON surface *in vivo*. PLS calibration was constructed using 21 data points correlated with the commercial glucometer. The validation plot was constructed using 5 data points. RMSEC = 7.46 mg/dL (0.41 mM) and RMSEP = 53.42 mg/dL (2.97 mM). $\lambda_{ex} = 785$ nm, $P = 50$ mW, and $t = 2$ min.

The calibration set was calculated using 21 data points. The validation set was constructed using five independent data points. The sensor showed a relatively low error (RMSEC = 7.46 mg/dL (0.41 mM) and RMSEP = 53.42 mg/dL (2.97 mM)).[60] The RMSEC and RMSEP can be improved by increasing the number of data points

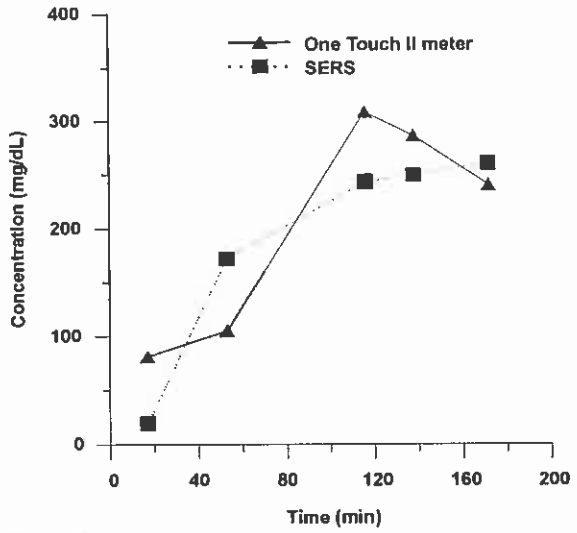

Figure 15.12 Comparison of *in vivo* glucose measurement using SERS and the One Touch II blood glucose meter. The glucose concentration change is plotted over time. Glucose bolus was started at $t = 60$ min. Squares (■■) are measurements made using the SERS sensor and triangles (▲) are measurements made using One Touch II blood glucose meter. $\lambda_{ex} = 785$ nm, $P = 50$ mW, and $t = 2$ min.

in the calibration set and by optimizing the substrate. These data compare favorably with existing detection methods, which have instrument-dependant coefficients of variation of 0.96–26.9% (0.096–2.69 mM, 1.75–49 mg/dL at 10 mM), as well as with our *in vitro* results.

In addition, to plot the data against the Clarke error grid, it is important to directly compare the SERS-based glucose sensor to a commercially available glucose sensor. Glucose concentration was measured in the rat using both the DT/MH AgFON SERS sensor and the One Touch II blood glucose meter. The data were plotted with respect to time and is shown in Figure15.12. Both the SERS-based measurements and the standard glucometer effectively tracked the sharp rise in glucose concentration after the start of the glucose infusion ($t = 60$ min) as well as subsequent changes in glucose concentration.[60]

15.4 CONCLUSIONS

The automatic and continuous monitoring of glucose levels is critically important for the care and treatment of millions of diabetics, particularly juvenile cases where observance of a strict medical regimen is often problematic. With further refinement of the system (e.g., instrumentation, optics, and surface), the SERS-based glucose sensor has the potential to replace conventional personal and point-of-care systems. The Raman spectrometer currently used for developing this sensor consists of a number of discrete components (laser, delivery optics, collection optics, spectrograph, and detector) that fit on 4 ft × 10 ft optical table and weighs a few hundred pounds. In order for the sensor to be used routinely in a clinical setting, the current spectrometer needs to be miniaturized. Several smaller Raman spectrometers have been developed that are paving the way for substantial miniaturization in the future. Small Raman systems that are now commercially available include Inspector Raman, a handheld system from DeltaNu with dimensions (6.5 × 4.5 × 2.5 in.), and a miniature 785 nm optimized spectrograph developed by Acton Instruments with dimensions 14 × 9.2 × 5.3 in. DeltaNu has also developed a second-generation handheld Raman spectrometer known as the ReporteR, which is palm-sized spectrometer (6 × 3 × 1.75 in.) and only weighs 11 oz. In addition, the Van Duyne group has made initial steps toward a miniature Raman system by replacing components of a laboratory-scale Raman system with smaller commercially available components. This system successfully collected Raman spectra using a laser pointer as the excitation source and a reflectance probe fiber-optic cable for laser delivery and collection.[70] Finally, Ondax, Inc. has fabricated a specialized 1 in. multiline filter that only allows certain wavelengths of light to pass through. This reduces the amount of noise that is collected and increases efficiency by giving the same signal to noise with a factor of 1.8 less collection time.[71] Combining this multiline filter with a notch filter to reject the laser light would produce an analyte-specific sensor. In addition, the development of an implantable sensor usable transdermally, where both the excitation and Stokes-shifted photons pass directly through the skin, will minimize the invasiveness of the procedure. Looking to the future, we predict that the functionalized SERS sensor approach will have important applications in both the treatment and the care of diabetes and will open up new areas of fundamental research.

ACKNOWLEDGMENTS

Funding for this work was provided by the NIH (5 R56 DK078691-02) and the U.S. Army Medical Research and Material Command's Military Operational Medical Research Program/Julia Weaver Fund (W81XWH-04-1-0630), and the NSF (CHE0414554).

REFERENCES

1. Cameron BD, Gorde HW, Satheesan B, Cote GL. The use of polarized laser light through the eye for noninvasive glucose monitoring. *Diabetes Technology & Therapeutics* 1999, 1, 125–143.
2. Malin SF, Ruchti TL, Blank TB, Thennadil SN, Monfre SL. Noninvasive prediction of glucose by near-infrared diffuse reflectance spectroscopy. *Clinical Chemistry* 1999, 45, 1651–1658.
3. Arnold MA. Progress in noninvasive glucose monitoring with near infrared transmission spectroscopy. *Abstracts of Papers of the American Chemical Society* 2002, 224, U114–U114.
4. Arnold FH, Zheng W, Michaels AS. A membrane-moderated, conductimetric sensor for the detection and measurement of specific organic solutes in aqueous solutions. *Journal of Membrane Science* 2000, 167, 227–239.
5. Asher SA, Alexeev VL, Goponenko AV, Sharma AC, Lednev IK, Wilcox CS, Finegold DN. Photonic crystal carbohydrate sensors: low ionic strength sugar sensing. *Journal of the American Chemical Society* 2003, 125, 3322–3329.
6. Cao YC, Jin RC, Nam JM, Thaxton CS, Mirkin CA. Raman dye-labeled nanoparticle probes for proteins. *Journal of the American Chemical Society* 2003, 125, 14676–14677.
7. Doering WE, Nie S. Single-molecule and single-nanoparticle SERS: examining the roles of surface active sites and chemical enhancement. *Journal of Physical Chemistry B* 2001, 106, 311–317.
8. Ni J, Lipert RJ, Dawson GB, Porter MD. Immunoassay readout method using extrinsic Raman labels adsorbed on immunogold colloids. *Analytical Chemistry* 1999, 71, 4903–4908.
9. McCreery RL. *Raman Spectroscopy for Chemical Analysis*, Vol. 157. John Wiley & Sons, Inc., New York, 2000, p. 420.
10. Lambert J, Storrie-Lombardi M, Borchert M. Measurement of physiologic glucose levels using Raman spectroscopy on a rabbit aqueous humor model. *IEEE LEOS Newsletter* 1998, 12, 19–22.
11. Berger AJ, Koo TW, Itzkan I, Horowitz G, Feld MS. Multicomponent blood analysis by near-infrared Raman spectroscopy. *Applied Optics* 1999, 38, 2916–2926.
12. American National Standard for the Safe Use of Lasers: ANSI Z-136. http://www.inform.umd.edu/PRES/policies/vi1600a.html.
13. Bell AF, Barron LD, Hecht L. Vibrational Raman optical activity study of D-Glucose. *Carbohydrate Research* 1994, 257, 11–24.

14. Chaiken J, Finney WF, Yang X, Knudson PE, Peterson KP, Peterson CM, Weinstock RS, Hagrman D. Progress in the noninvasive, *in-vivo*, tissue modulated Raman spectroscopy of human blood. *Proceedings of SPIE* 2001, 4254, 216–227.
15. Van Duyne RP. Applications of Raman spectroscopy in electrochemistry. *Journal of Physique* 1977, 38, (C5)239–(C5)252.
16. Campion A, Kambhampati P. Surface-enhanced Raman scattering. *Chemical Society Reviews* 1998, 27, 241–250.
17. Kneipp K, Wang Y, Kneipp H, Perelman LT, Itzkan I, Dasari RR, Feld MS. Single molecule detection using surface-enhanced Raman scattering (SERS). *Physical Review Letters* 1997, 78, 1667–1670.
18. Nie S, Emory SR. Probing single molecules and single nanoparticles by surface-enhanced Raman scattering. *Science* 1997, 275, 1102–1106.
19. Haynes CL, Van Duyne RP. Plasmon-sampled surface-enhanced Raman excitation spectroscopy. *Journal of Physical Chemistry B* 2003, 107, 7426–7433.
20. Schatz GC, Van Duyne RP. Electromagnetic mechanism of surface-enhanced spectroscopy. In: Chalmers JM, Griffiths PR (Eds), *Handbook of Vibrational Spectroscopy*, Vol. 1. John Wiley & Sons, Ltd, Chichester, 2002, pp. 759–774.
21. Flaugh PL, O'Donnell SE, Asher SA. Development of a new optical wavelength rejection filter: demonstration of its utility in Raman spectroscopy. *Applied Spectroscopy* 1984, 38, 847–850.
22. Munro CH, Pajcini V, Asher SA. Dielectric stack filters for *ex situ* and *in situ* UV optical-fiber probe Raman spectroscopic measurements. *Applied Spectroscopy* 1997, 51, 1722–1729.
23. Emory SR, Haskins WE, Nie S. Direct observation of size-dependent optical enhancement in single metal nanoparticles. *Journal of the American Chemical Society* 1998, 120, 8009–8010.
24. Emory SR, Nie S. Screening and enrichment of metal nanoparticles with novel optical properties. *Journal of Physical Chemistry B* 1998, 102, 493–497.
25. Kahl M, Voges E, Kostrewa S, Viets C, Hill W. Periodically structured metallic substrates for SERS. *Sensors and Actuators B: Chemical* 1998, 51, 285–291.
26. Yang WH, Hulteen JC, Schatz GC, Van Duyne RP. A surface-enhanced hyper-Raman and surface-enhanced Raman scattering study of *trans*-1,2-bis(4-pyridyl)ethylene adsorbed onto silver film over nanosphere electrodes. Vibrational assignments: experiment and theory. *Journal of Chemical Physics* 1996, 104, 4313–4323.
27. Pipino ACR, Schatz GC, Van Duyne RP. Surface-enhanced second-harmonic diffraction: experimental investigation of selective enhancement. *Physical Review B* 1996, 53, 4162–4169.
28. Zhu J, Xu F, Schofer SJ, Mirkin CA. The first Raman spectrum of an organic monolayer on a high-temperature superconductor: direct spectroscopic evidence for a chemical interaction between an amine and $YBa_2Cu_3O_{7-\delta}$. *Journal of the American Chemical Society* 1997, 119, 235–236.
29. Freeman RG, Grabar KC, Allison KJ, Bright RM, Davis JA, Guthrie AP, Hommer MB, Jackson MA, Smith PC, Walter DG, Natan MJ. Self-assembled metal colloid monolayers: an approach to SERS substrates. *Science* 1995, 267, 1629–1632.
30. Caldwell WB, Chen K, Herr BR, Mirkin CA, Hulteen JC, Van Duyne RP. Self-assembled monolayers of ferrocenylazobenzenes on Au(111)/mica films: surface-enhanced Raman scattering (SERS) response vs. surface morphology. *Langmuir* 1994, 10, 4109–4115.

31. Van Duyne RP, Hulteen JC, Treichel DA. Atomic force microscopy and surface-enhanced Raman spectroscopy. I. Ag island films and Ag film over polymer nanosphere surfaces supported on glass. *Journal of Chemical Physics* 1993, 99, 2101–2115.
32. Liao PF. Silver structures produced by microlithography. In: Chang RK, Furtak TE (Eds), *Surface Enhanced Raman Scattering*. Plenum Press, New York, 1982, pp. 379–390.
33. Liao PF, Bergman JG, Chemla DS, Wokaun A, Melngailis J, Hawryluk AM, Economou NP. Surface-enhanced Raman scattering from microlithographic silver particle surfaces. *Chemical Physics Letters* 1981, 81, 355–359.
34. Howard RE, Liao PF, Skocpol WJ, Jackel LD, Craighead HG. Microfabrication as a scientific tool. *Science* 1983, 221, 117–121.
35. Elghanian R, Storhoff JJ, Mucic RC, Letsinger RL, Mirkin CA. Selective colorimetric detection of polynucleotides based on the distance-dependent optical properties of gold nanoparticles. *Science* 1997, 277, 1078–1081.
36. Mucic RC, Storhoff JJ, Letsinger RL, Mirkin CA. DNA-induced assembly of gold nanoparticles: a method for rationally organizing colloidal particles into ordered macroscopic materials. *Nature* 1996, 382, 607–609.
37. Storhoff JJ, Elghanian R, Mucic RC, Mirkin CA, Letsinger RL. One-pot colorimetric differentiation of polynucleotides with single base imperfections using gold nanoparticle probes. *Journal of the American Chemical Society* 1998, 120, 1959–1964.
38. BruchezJrM, Moronne M, Gin P, Weiss S, Alivisatos AP. Semiconductor nanocrystals as fluorescent biological labels. *Science* 1998, 281, 2013–2018.
39. Chan WCW, Nie S. Quantum dot bioconjugates for ultrasensitive nonisotopic detection. *Science* 1998, 281, 2016–2018.
40. Pan G, Kesavamoorthy R, Asher SA. Nanosecond switchable polymerized crystalline colloidal array Bragg diffracting materials. *Journal of the American Chemical Society* 1998, 120, 6525–6530.
41. Weissman JM, Sunkara HB, Tse AS, Asher SA. Thermally switchable periodicities and diffraction from mesoscopically ordered materials. *Science* 1996, 274, 959–960.
42. Asher S, Chang S-Y, Tse A, Liu L, Pan G, Wu Z, Li P. Optically nonlinear crystalline colloidal self assembled submicron periodic structures for optical limiters. *Material Research Society Symposium Proceedings* 1995, 374, 305–310.
43. Lidorikis E, Li Q, Soukoulis CM. Optical bistability in colloidal crystals. *Physical Review E* 1997, 55, 3613–3618.
44. Mansour K, Soileau MJ, Van Stryland EW. Nonlinear optical properties of carbon-black suspensions (ink). *Journal of the Optical Society of America B* 1992, 9, 1100–1109.
45. Woileau MJ. Materials for optical switches, isolators, and limiters. *Proceedings of SPIE* 1989, 1105, 187.
46. Haynes CL, Van Duyne RP. Nanosphere lithography: a versatile nanofabrication tool for studies of size-dependent nanoparticle optics. *Journal of Physical Chemistry B* 2001, 105, 5599–5611.
47. McFarland AD, Young MA, Dieringer JA, Van Duyne RP. Wavelength-scanned surface-enhanced Raman excitation spectroscopy. *Journal of Physical Chemistry B* 2005, 109, 11279–11285.
48. Hulteen JC, Van Duyne RP. Nanosphere lithography: a materials general fabrication process for periodic particle array surfaces. *Journal of Vacuum Science and Technology A* 1995, 13, 1553–1558.

49. Haynes CL, Van Duyne R. Plasmon scanned surface-enhanced Raman scattering excitation profiles. *Material Research Society Symposium Proceedings* 2002, 728, S10.7.1–S10.7.6.

50. Smith WE, RodgerC. Surface-enhanced Raman scattering. In: Chalmers JM, Griffiths PR (Eds), *Handbook of Vibrational Spectroscopy*, Vol. 1. John Wiley & Sons, Chichester, UK, 2002, pp. 775–784.

51. Freunscht P, Van Duyne RP, Schneider S. Surface-enhanced Raman spectroscopy of *trans*-stilbene adsorbed on silver film over nanosphere surfaces modified by platinum or alkanethiol deposition. *Chemical Physics Letters* 1997, 281, 372–378.

52. Blanco Gomis D, Tamayo DM, Mangas Alonso J. Determination of monosaccharides in cider by reversed-phase liquid chromatography. *Analytica Chimica Acta* 2001, 436, 173.

53. Yang L, Janle E, Huang T, Gitzen J, Kissinger PT, Vreeke M, Heller A. Applications of "wired" peroxidase electrodes for peroxide determination in liquid chromatography coupled to oxidase immobilized enzyme reactors. *Analytical Chemistry* 1995, 34, 1326–1331.

54. Carron KT, Kennedy BJ. Molecular-specific chromatographic detector using modified SERS substrates. *Analytical Chemistry* 1995, 67, 3353–3356.

55. Deschaines TO, Carron KT. Stability and surface uniformity of selected thiol-coated SERS surfaces. *Applied Spectroscopy* 1997, 51, 1355–1359.

56. Shafer-Peltier KE, Haynes CL, Glucksberg MR, Van Duyne RP. Toward a glucose biosensor on surface-enhanced Raman scattering. *Journal of the American Chemical Society* 2003, 125, 588–593.

57. Yonzon CR, Haynes CL, Zhang XY, Walsh JT, Van Duyne RP. A glucose biosensor based on surface-enhanced Raman scattering: improved partition layer, temporal stability, reversibility, and resistance to serum protein interference. *Analytical Chemistry* 2004, 76, 78–85.

58. Lyandres O, Shah NC, Yonzon CR, Walsh JT, Glucksberg MR, Van Duyne RP. Real-time glucose sensing by surface-enhanced Raman spectroscopy in bovine plasma facilitated by a mixed decanethiol/mercaptohexanol partition layer. *Analytical Chemistry* 2005, 77, 6134–6139.

59. Zhang X, Young MA, Lyandres O, Van Duyne RP. Rapid detection of an anthrax biomarker by surface-enhanced Raman spectroscopy. *Journal of the American Chemical Society* 2005, 127, 4484–4489.

60. Stuart DA, Yuen JM, Shah NC, Lyandres O, Yonzon CR, Glucksberg MR, Walsh JT, Van Duyne RP. *In vivo* glucose measurement by surface-enhanced Raman spectroscopy. *Analytical Chemistry* 2006, 78, 7211–7215.

61. Beebe KR, Pell RJ, Seasholtz MB. *Chemometrics: A Practical Guide*, Wiley Interscience, New York, 1998, p. 348.

62. Junod A, Lambert AE, Stauffac W, Renold AE. Diabetogenic action of streptozotocin: relationship of dose to metabolic response. *Journal of Clinical Investigation* 1969, 48, 2129–2139.

63. Mosier-Boss PA, Lieberman SH. Detection of nitrate and sulfate anions by normal Raman spectroscopy and SERS of cationic-coated, silver substrates. *Applied Spectroscopy* 2000, 54, 1126–1135.

64. Soderholm S, Roos YH, Meinander N, Hotokka M. Raman spectra of fructose and glucose in the amorphous and crystalline states. *Journal of Raman Spectroscopy* 1999, 30, 1009–1018.

65. Stacy AM, Van Duyne RP. Surface enhanced Raman and resonance Raman spectroscopy in a non-aqueous electrochemical environment: tris(2,2′-bipyridine)ruthenium(II) adsorbed on silver from acetonitrile. *Chemical Physics Letters* 1983, 102, 365–370.

66. Kaufman FR, Gibson LC, Halvorson M, Carpenter S, Fisher LK, Pitukcheewanont P. A pilot study of the continuous glucose monitoring system: clinical decisions and glycemic control after its use in pediatric type 1 diabetic subjects. *Diabetes Care* 2001, 24, 2030–2034.

67. Stuart DA, Yonzon CR, Zhang X, Lyandres O, Shah NC, Glucksberg MR, Walsh JT, Van Duyne RP. Glucose sensing using near infrared surface-enhanced Raman spectroscopy: gold surfaces, 10-day stability, and improved accuracy. *Analytical Chemistry* 2005, 77, 4013–4019.

68. Bryant MA, Pemberton JE. Surface Raman-scattering of self-assembled monolayers formed from 1-alkanethiols – behavior of films at Au and comparison to films at Ag. *Journal of the American Chemical Society* 1991, 113, 8284–8293.

69. Biebuyck HA, Bain CD, Whitesides GM. Comparison of organic monolayers on polycrystalline gold spontaneously assembled from solutions containing dialkyl disulfides or alkanethiols. *Langmuir* 1994, 10, 1825–1831.

70. Young MA, Stuart DA, Lyandres O, Glucksberg MR, Van Duyne RP. Surface-enhanced Raman spectroscopy with a laser pointer light source and miniature spectrometer. *Canadian Journal of Chemistry* 2004, 82, 1435–1441.

71. Caltech Astronomy: Holographic Filter Allows Astronomers to Read between the Lines. http://www.astro.caltech.edu/palomar/ohfilter.html (accessed on June 25, 2008).